

SIMPLE IMPLEMENTATION OF ARBITRARILY SHAPED TOTAL-FIELD/SCATTERED-FIELD REGIONS IN FINITE-DIFFERENCE FREQUENCY-DOMAIN

R. C. Rumpf*

EM Lab, W. M. Keck Center for 3D Innovation, University of Texas at El Paso, USA

Abstract—The total-field/scattered-field (TF/SF) formulation is a popular technique for incorporating sources into electromagnetic models like the finite-difference frequency-domain (FDFD) method. It is versatile and simplifies calculation of waves scattered from a device. In the context of FDFD, the TF/SF formulation involves modifying all of the finite-difference equations that contain field terms from both the TF and SF regions in order to make the terms compatible. While simple in concept, modifying all of the equations for arbitrarily shaped TF/SF regions is tedious and no solution has been offered in the literature to do it in a straightforward manner. This paper presents a simple and efficient technique for implementing the TF/SF formulation that allows the TF/SF regions to be any shape and of arbitrary complexity. Its simplicity and versatility are demonstrated by giving several practical examples including a diffraction grating, a waveguide problem, and a scattering problem with a cylindrical wave source.

1. INTRODUCTION

The finite-difference frequency-domain (FDFD) method may be the easiest of all rigorous numerical techniques to implement [1–4]. It is a fully numerical method that is excellent for field visualization and modeling structures with complex geometries or devices of finite size. It is accurate, stable, and the sources of error are well understood. Being a frequency-domain method, it is able to resolve sharp resonances and obtain solutions at a single frequency more efficiently than time-domain methods. It is able to account for oblique angle of incidence

Received 20 September 2011, Accepted 28 October 2011, Scheduled 10 November 2011

* Corresponding author: Raymond C. Rumpf (rcrumpf@utep.edu).

and incorporate material dispersion more easily than time-domain methods. The method works by transforming Maxwell's equations into a set of linear algebraic equations using the finite-difference method. This large set of equations is written in matrix form as $\mathbf{Ax}=\mathbf{0}$ where \mathbf{A} is the wave matrix and \mathbf{x} is the field to be calculated. This equation has only a trivial solution so it cannot be solved without incorporating a source vector \mathbf{b} to put the matrix equation in the form of $\mathbf{Ax}=\mathbf{b}$. Given this second matrix equation, the field is calculated by solving $\mathbf{x}=\mathbf{A}^{-1}\mathbf{b}$.

Calculating the source vector \mathbf{b} is not an intuitive or obvious process, particularly for those new to numerical modeling. A simple and powerful equation is derived in this paper to calculate the source vector using the total-field/scattered-field (TF/SF) technique [5–7]. Without this equation, TF/SF can be a cumbersome and confusing technique to implement. In the TF/SF framework, the grid is divided into two regions; the total-field (TF) and the scattered-field (SF) regions. The TF region is the physically real region and contains both the source and the waves scattered from a device. The SF region is a non-physical mathematically constructed region that contains only the scattered waves and not the source. The TF/SF formulation can be used to minimize energy incident of absorbing boundary conditions as well as to automatically separate the source from the scattered-field. This second feature makes calculation of quantities like transmittance and reflectance easier during post-processing.

This paper is organized as follows. First, the standard formulation of the FDFD method is presented in order to calculate a wave matrix \mathbf{A} . Second, the derivation is presented of the equation used to calculate the source vector \mathbf{b} based on the TF/SF technique. Third, the general implementation of the FDFD method using this equation is presented. Finally, several practical examples are given before the paper is concluded.

2. FORMULATION OF THE STANDARD FINITE-DIFFERENCE FREQUENCY-DOMAIN METHOD

The grid schemes for two typical FDFD problems are illustrated in Figure 1. At left is a 2D grid to model scattering from a finite device. It is surrounded by a perfectly matched layer (PML) on all four sides to absorb outgoing waves in all directions [8–11]. The TF/SF method is used to inject a source and to minimize energy incident on the absorbing boundaries by removing the source in those regions. Near the boundary of the PML, the dashed line highlights the interface

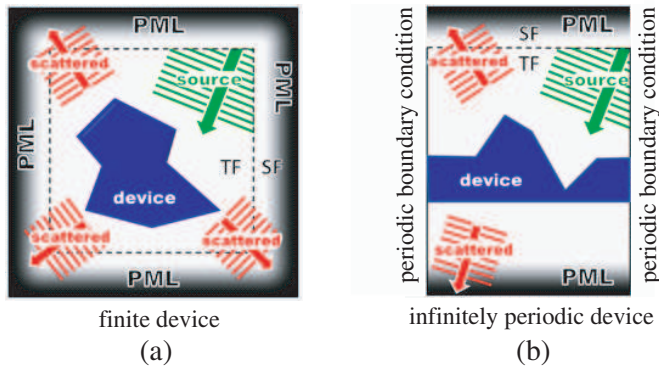


Figure 1. (a) FDFD grid scheme to model scattering from a finite device. (b) FDFD grid scheme to model transmission and reflection from a periodic structure.

between the TF and SF regions. The waves scattered from the device are free to pass through the TF/SF interface and into the SF region where they are recorded and then absorbed by the PML. When post-processing the scattered fields, it is not necessary to separate the source from the scattered waves because this is handled automatically by the TF/SF framework. Figure 1(b) shows the typical grid scheme used to model scattering from periodic structures like metamaterials, gratings, and frequency selective surfaces. Here, a PML is only used at the top and bottom parts of the grid because periodic boundary conditions are used on the left and right boundaries of the grid. In this configuration, the SF region resides solely at the top of the grid and the TF/SF formulation can be thought of as a way of injecting a “one-way source” toward the device from above. No power is launched in the backward direction away from the device.

2.1. Maxwell’s Equations with a Perfectly Matched Layer

Formulation of the FDFD method begins with Maxwell’s curl equations [12]. After normalizing the magnetic field according to $\vec{H} = -j\eta_0\vec{H}$, Maxwell’s curl equations with a uniaxial PML (UPML) can be written as

$$\nabla \times \vec{E} = k_0[\mu_r][s]\vec{H} \tag{1}$$

$$\nabla \times \vec{H} = k_0[\varepsilon_r][s]\vec{E} \tag{2}$$

For a UPML, the tensor $[s]$ is expressed as

$$[s] = \begin{bmatrix} \frac{s_y s_z}{s_x} & 0 & 0 \\ 0 & \frac{s_x s_z}{s_y} & 0 \\ 0 & 0 & \frac{s_x s_y}{s_z} \end{bmatrix} \quad (3)$$

One effective way to calculate the PML terms in Eq. (3) is

$$s_x(x) = s_{x0}(x) [1 - j\eta_0 \sigma'_x(x)] \quad s_{x0}(x) = 1 + s_{\max} \cdot \left(\frac{x}{L_x}\right)^p$$

$$\sigma'_x(x) = \sigma'_{\max} \sin^2\left(\frac{\pi x}{2L_x}\right) \quad (4)$$

$$s_y(y) = s_{y0}(y) [1 - j\eta_0 \sigma'_y(y)] \quad s_{y0}(y) = 1 + s_{\max} \cdot \left(\frac{y}{L_y}\right)^p$$

$$\sigma'_y(y) = \sigma'_{\max} \sin^2\left(\frac{\pi y}{2L_y}\right) \quad (5)$$

$$s_z(z) = s_{z0}(z) [1 - j\eta_0 \sigma'_z(z)] \quad s_{z0}(z) = 1 + s_{\max} \cdot \left(\frac{z}{L_z}\right)^p$$

$$\sigma'_z(z) = \sigma'_{\max} \sin^2\left(\frac{\pi z}{2L_z}\right) \quad (6)$$

Typical values for the various parameters above are $1 \leq p < 5$, $0 \leq s_{\max} \leq 5$, and $\sigma'_{\max} = 1$. The prime superscript on the σ' terms indicates that these are purely fictitious conductivity terms separate from the physical conductivity that is usually accounted for in a complex dielectric constant. The typical number of cells for a PML ranges between 10 and 40. The parameters L_x , L_y , and L_z are the physical lengths of the PML so that the ratios x/L_x , y/L_y and z/L_z increase from zero to one moving through the PML from the center of the grid. When the tensor quantities $[\mu_r]$ and $[\varepsilon_r]$ are restricted to be diagonal, Eqs. (1) and (2) can be expanded into the following set of six coupled partial differential equations.

$$\frac{\partial E_z}{\partial y'} - \frac{\partial E_y}{\partial z'} = \mu_{xx} \frac{s_y s_z}{s_x} \tilde{H}_x \quad (7)$$

$$\frac{\partial E_x}{\partial z'} - \frac{\partial E_z}{\partial x'} = \mu_{yy} \frac{s_x s_z}{s_y} \tilde{H}_y \quad (8)$$

$$\frac{\partial E_y}{\partial x'} - \frac{\partial E_x}{\partial y'} = \mu_{zz} \frac{s_x s_y}{s_z} \tilde{H}_z \quad (9)$$

$$\frac{\partial \tilde{H}_z}{\partial y'} - \frac{\partial \tilde{H}_y}{\partial z'} = \varepsilon_{xx} \frac{s_y s_z}{s_x} E_x \quad (10)$$

$$\frac{\partial \tilde{H}_x}{\partial z'} - \frac{\partial \tilde{H}_x}{\partial x'} = \epsilon_{yy} \frac{s_x s_z}{s_y} E_y \tag{11}$$

$$\frac{\partial \tilde{H}_y}{\partial x'} - \frac{\partial \tilde{H}_x}{\partial y'} = \epsilon_{zz} \frac{s_x s_y}{s_z} E_z \tag{12}$$

Here, the grid coordinates have been normalized according to

$$x' = k_0 x \quad y' = k_0 y \quad z' = k_0 z \tag{13}$$

2.2. Finite-Difference Approximation of Maxwell's Equations

The derivatives in Maxwell's equations can be approximated using central finite-differences where the fields and materials are assigned to discrete points on a Yee grid [13, 14]. This arrangement staggers the field components within each cell of the grid so that all of the electric field components are encircled by magnetic field components and all of the magnetic field components are encircled by electric field components. The Yee cells for 1D, 2D, and 3D grids are illustrated in Figure 2. This staggered arrangement provides an efficient means to approximate the curl operations by finite-differences. In addition, the physical boundary conditions are naturally satisfied and Maxwell's divergence equations are implicitly satisfied so spurious solutions are avoided [14].

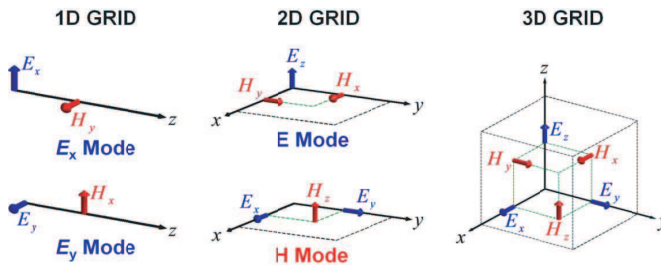


Figure 2. The Yee grid scheme for 1D, 2D, and 3D formulations.

After approximating the derivatives in Maxwell's equations with central finite-differences on a Yee grid, Eqs. (7)–(12) become

$$\frac{E_z^{(i-\frac{1}{2}, j+\frac{3}{2}, k+1)} - E_z^{(i-\frac{1}{2}, j+\frac{1}{2}, k+1)}}{\Delta y'} - \frac{E_y^{(i-\frac{1}{2}, j+1, k+\frac{3}{2})} - E_y^{(i-\frac{1}{2}, j+1, k+\frac{1}{2})}}{\Delta z'} = \mu_{xx}^{(i-\frac{1}{2}, j+1, k+1)} \frac{s_y^{(i-\frac{1}{2}, j+1, k+1)} s_z^{(i-\frac{1}{2}, j+1, k+1)}}{s_x^{(i-\frac{1}{2}, j+1, k+1)}} \tilde{H}_x^{(i-\frac{1}{2}, j+1, k+1)} \tag{14}$$

$$\begin{aligned} & \frac{E_x^{(i,j+\frac{1}{2},k+\frac{3}{2})} - E_x^{(i,j+\frac{1}{2},k+\frac{1}{2})}}{\Delta z'} - \frac{E_z^{(i+\frac{1}{2},j+\frac{1}{2},k+1)} - E_z^{(i-\frac{1}{2},j+\frac{1}{2},k+1)}}{\Delta x'} \\ &= \mu_{yy} \frac{s_x^{(i,j+\frac{1}{2},k+1)} s_z^{(i,j+\frac{1}{2},k+1)}}{s_y^{(i,j+\frac{1}{2},k+1)}} \tilde{H}_y^{(i,j+\frac{1}{2},k+1)} \end{aligned} \quad (15)$$

$$\begin{aligned} & \frac{E_y^{(i+\frac{1}{2},j+1,k+\frac{1}{2})} - E_y^{(i-\frac{1}{2},j+1,k+\frac{1}{2})}}{\Delta x'} - \frac{E_x^{(i,j+\frac{3}{2},k+\frac{1}{2})} - E_x^{(i,j+\frac{1}{2},k+\frac{1}{2})}}{\Delta y'} \\ &= \mu_{zz} \frac{s_x^{(i,j+1,k+\frac{1}{2})} s_y^{(i,j+1,k+\frac{1}{2})}}{s_z^{(i,j+1,k+\frac{1}{2})}} \tilde{H}_z^{(i,j+1,k+\frac{1}{2})} \end{aligned} \quad (16)$$

$$\begin{aligned} & \frac{\tilde{H}_z^{(i,j+1,k+\frac{1}{2})} - \tilde{H}_z^{(i,j,k+\frac{1}{2})}}{\Delta y'} - \frac{\tilde{H}_y^{(i,j+\frac{1}{2},k+1)} - \tilde{H}_y^{(i,j+\frac{1}{2},k)}}{\Delta z'} \\ &= \varepsilon_{xx} \frac{s_y^{(i,j+\frac{1}{2},k+\frac{1}{2})} s_z^{(i,j+\frac{1}{2},k+\frac{1}{2})}}{s_x^{(i,j+\frac{1}{2},k+\frac{1}{2})}} E_x^{(i,j+\frac{1}{2},k+\frac{1}{2})} \end{aligned} \quad (17)$$

$$\begin{aligned} & \frac{\tilde{H}_x^{(i-\frac{1}{2},j+1,k+1)} - \tilde{H}_x^{(i-\frac{1}{2},j+1,k)}}{\Delta z'} - \frac{\tilde{H}_z^{(i,j+1,k+\frac{1}{2})} - \tilde{H}_z^{(i-1,j+1,k+\frac{1}{2})}}{\Delta x'} \\ &= \varepsilon_{yy} \frac{s_x^{(i-\frac{1}{2},j+1,k+\frac{1}{2})} s_z^{(i-\frac{1}{2},j+1,k+\frac{1}{2})}}{s_y^{(i-\frac{1}{2},j+1,k+\frac{1}{2})}} E_y^{(i-\frac{1}{2},j+1,k+\frac{1}{2})} \end{aligned} \quad (18)$$

$$\begin{aligned} & \frac{\tilde{H}_y^{(i,j+\frac{1}{2},k+1)} - \tilde{H}_y^{(i-1,j+\frac{1}{2},k+1)}}{\Delta x'} - \frac{\tilde{H}_x^{(i-\frac{1}{2},j+1,k+1)} - \tilde{H}_x^{(i-\frac{1}{2},j,k+1)}}{\Delta y'} \\ &= \varepsilon_{zz} \frac{s_x^{(i-\frac{1}{2},j+\frac{1}{2},k+1)} s_y^{(i-\frac{1}{2},j+\frac{1}{2},k+1)}}{s_z^{(i-\frac{1}{2},j+\frac{1}{2},k+1)}} E_z^{(i-\frac{1}{2},j+\frac{1}{2},k+1)} \end{aligned} \quad (19)$$

Each of these equations is written once for every cell in the grid so each finite-difference equation produces a large set of linear algebraic equations that can be written in matrix form as

$$\mathbf{D}_{y'}^e \mathbf{e}_z - \mathbf{D}_{z'}^e \mathbf{e}_y = \boldsymbol{\mu}_{xx} \tilde{\mathbf{h}}_x \quad (20)$$

$$\mathbf{D}_{z'}^e \mathbf{e}_x - \mathbf{D}_{x'}^e \mathbf{e}_z = \boldsymbol{\mu}_{yy} \tilde{\mathbf{h}}_y \quad (21)$$

$$\mathbf{D}_{x'}^e \mathbf{e}_y - \mathbf{D}_{y'}^e \mathbf{e}_x = \boldsymbol{\mu}_{zz} \tilde{\mathbf{h}}_z \quad (22)$$

$$\mathbf{D}_{y'}^h \tilde{\mathbf{h}}_z - \mathbf{D}_{z'}^h \tilde{\mathbf{h}}_y = \boldsymbol{\varepsilon}_{xx} \mathbf{e}_x \quad (23)$$

$$\mathbf{D}_{z'}^h \tilde{\mathbf{h}}_x - \mathbf{D}_{x'}^h \tilde{\mathbf{h}}_z = \boldsymbol{\varepsilon}_{yy} \mathbf{e}_y \quad (24)$$

$$\mathbf{D}_{x'}^h \tilde{\mathbf{h}}_y - \mathbf{D}_{y'}^h \tilde{\mathbf{h}}_x = \boldsymbol{\varepsilon}_{zz} \mathbf{e}_z \tag{25}$$

The terms \mathbf{e}_x , \mathbf{e}_y , \mathbf{e}_z , $\tilde{\mathbf{h}}_x$, $\tilde{\mathbf{h}}_y$ and $\tilde{\mathbf{h}}_z$ are column vectors that contain all of the field components throughout the entire grid reshaped into linear arrays.

$$\mathbf{e}_x = \begin{bmatrix} E_x^{(\frac{1}{2},0,0)} \\ E_x^{(\frac{3}{2},0,0)} \\ \vdots \\ E_x^{(N_x-\frac{1}{2},N_y-1,N_z-1)} \end{bmatrix} \quad \mathbf{e}_y = \begin{bmatrix} E_y^{(0,\frac{1}{2},0)} \\ E_y^{(1,\frac{1}{2},0)} \\ \vdots \\ E_y^{(N_x-1,N_y-\frac{1}{2},N_z-1)} \end{bmatrix}$$

$$\mathbf{e}_z = \begin{bmatrix} E_z^{(0,0,\frac{1}{2})} \\ E_z^{(1,0,\frac{1}{2})} \\ \vdots \\ E_z^{(N_x-1,N_y-1,N_z-\frac{1}{2})} \end{bmatrix} \tag{26}$$

$$\tilde{\mathbf{h}}_x = \begin{bmatrix} \tilde{H}_x^{(0,\frac{1}{2},\frac{1}{2})} \\ \tilde{H}_x^{(1,\frac{1}{2},\frac{1}{2})} \\ \vdots \\ \tilde{H}_x^{(N_x-1,N_y-\frac{1}{2},N_z-\frac{1}{2})} \end{bmatrix} \quad \tilde{\mathbf{h}}_y = \begin{bmatrix} \tilde{H}_y^{(\frac{1}{2},0,\frac{1}{2})} \\ \tilde{H}_y^{(\frac{3}{2},0,\frac{1}{2})} \\ \vdots \\ \tilde{H}_y^{(N_x-\frac{1}{2},N_y-1,N_z-\frac{1}{2})} \end{bmatrix}$$

$$\tilde{\mathbf{h}}_z = \begin{bmatrix} \tilde{H}_z^{(\frac{1}{2},\frac{1}{2},0)} \\ \tilde{H}_z^{(\frac{3}{2},\frac{1}{2},0)} \\ \vdots \\ \tilde{H}_z^{(N_x-\frac{1}{2},N_y-\frac{1}{2},N_z-1)} \end{bmatrix} \tag{27}$$

The terms $\mathbf{D}_{x'}^e$, $\mathbf{D}_{y'}^e$ and $\mathbf{D}_{z'}^e$ are banded matrices that calculate first-order spatial derivatives of the electric fields across the grid [15–18]. As a quick example of what these matrices look like, they were computed for a two-dimensional grid composed of only 4×4 cells. Using Dirichlet boundary conditions, the matrix derivative operators $\mathbf{D}_{x'}^e$ and $\mathbf{D}_{y'}^e$ for

In Eq. (30), the “ H ” superscript indicates a Hermitian transpose operation. Finally, the terms $\boldsymbol{\mu}_{xx}$, $\boldsymbol{\mu}_{yy}$, $\boldsymbol{\mu}_{zz}$, $\boldsymbol{\varepsilon}_{xx}$, $\boldsymbol{\varepsilon}_{yy}$, and $\boldsymbol{\varepsilon}_{zz}$ are diagonal matrices containing the relative permittivity throughout the grid. These perform point-by-point multiplication operations on the field terms. In addition, the PML terms have been absorbed into these quantities giving them the following general form where $\text{diag}[]$ is a procedure that reshapes a multidimensional function into a linear array and places that array along the diagonal of a sparse matrix.

$$\boldsymbol{\mu}_{xx} = \text{diag}[\mu_{xx} s_x^{-1} s_y s_z] \quad \boldsymbol{\mu}_{yy} = \text{diag}[\mu_{yy} s_x s_y^{-1} s_z] \quad \boldsymbol{\mu}_{zz} = \text{diag}[\mu_{zz} s_x s_y s_z^{-1}] \quad (31)$$

$$\boldsymbol{\varepsilon}_{xx} = \text{diag}[\varepsilon_{xx} s_x^{-1} s_y s_z] \quad \boldsymbol{\varepsilon}_{yy} = \text{diag}[\varepsilon_{yy} s_x s_y^{-1} s_z] \quad \boldsymbol{\varepsilon}_{zz} = \text{diag}[\varepsilon_{zz} s_x s_y s_z^{-1}] \quad (32)$$

2.3. Three-Dimensional Matrix Wave Equation

Equations (20)–(22) and Eqs. (23)–(25) can be written in block matrix form as

$$\begin{bmatrix} \mathbf{0} & -\mathbf{D}_{z'}^e & \mathbf{D}_{y'}^e \\ \mathbf{D}_{z'}^e & \mathbf{0} & -\mathbf{D}_{x'}^e \\ -\mathbf{D}_{y'}^e & \mathbf{D}_{x'}^e & \mathbf{0} \end{bmatrix} \begin{bmatrix} \mathbf{e}_x \\ \mathbf{e}_y \\ \mathbf{e}_z \end{bmatrix} = \begin{bmatrix} \boldsymbol{\mu}_{xx} & \mathbf{0} & \mathbf{0} \\ \mathbf{0} & \boldsymbol{\mu}_{yy} & \mathbf{0} \\ \mathbf{0} & \mathbf{0} & \boldsymbol{\mu}_{zz} \end{bmatrix} \begin{bmatrix} \tilde{\mathbf{h}}_x \\ \tilde{\mathbf{h}}_y \\ \tilde{\mathbf{h}}_z \end{bmatrix} \quad (33)$$

$$\begin{bmatrix} \mathbf{0} & -\mathbf{D}_{z'}^h & \mathbf{D}_{y'}^h \\ \mathbf{D}_{z'}^h & \mathbf{0} & -\mathbf{D}_{x'}^h \\ -\mathbf{D}_{y'}^h & \mathbf{D}_{x'}^h & \mathbf{0} \end{bmatrix} \begin{bmatrix} \tilde{\mathbf{h}}_x \\ \tilde{\mathbf{h}}_y \\ \tilde{\mathbf{h}}_z \end{bmatrix} = \begin{bmatrix} \boldsymbol{\varepsilon}_{xx} & \mathbf{0} & \mathbf{0} \\ \mathbf{0} & \boldsymbol{\varepsilon}_{yy} & \mathbf{0} \\ \mathbf{0} & \mathbf{0} & \boldsymbol{\varepsilon}_{zz} \end{bmatrix} \begin{bmatrix} \mathbf{e}_x \\ \mathbf{e}_y \\ \mathbf{e}_z \end{bmatrix} \quad (34)$$

A matrix wave equation for the electric field can be derived by solving Eq. (33) for the magnetic fields and substituting that expression into Eq. (34). The result is

$$\left\{ \begin{bmatrix} \mathbf{0} & -\mathbf{D}_{z'}^h & \mathbf{D}_{y'}^h \\ \mathbf{D}_{z'}^h & \mathbf{0} & -\mathbf{D}_{x'}^h \\ -\mathbf{D}_{y'}^h & \mathbf{D}_{x'}^h & \mathbf{0} \end{bmatrix} \begin{bmatrix} \boldsymbol{\mu}_{xx}^{-1} & \mathbf{0} & \mathbf{0} \\ \mathbf{0} & \boldsymbol{\mu}_{yy}^{-1} & \mathbf{0} \\ \mathbf{0} & \mathbf{0} & \boldsymbol{\mu}_{zz}^{-1} \end{bmatrix} \begin{bmatrix} \mathbf{0} & -\mathbf{D}_{z'}^e & \mathbf{D}_{y'}^e \\ \mathbf{D}_{z'}^e & \mathbf{0} & -\mathbf{D}_{x'}^e \\ -\mathbf{D}_{y'}^e & \mathbf{D}_{x'}^e & \mathbf{0} \end{bmatrix} - \begin{bmatrix} \boldsymbol{\varepsilon}_{xx} & \mathbf{0} & \mathbf{0} \\ \mathbf{0} & \boldsymbol{\varepsilon}_{yy} & \mathbf{0} \\ \mathbf{0} & \mathbf{0} & \boldsymbol{\varepsilon}_{zz} \end{bmatrix} \right\} \begin{bmatrix} \mathbf{e}_x \\ \mathbf{e}_y \\ \mathbf{e}_z \end{bmatrix} = \begin{bmatrix} \mathbf{0} \\ \mathbf{0} \\ \mathbf{0} \end{bmatrix} \quad (35)$$

Similarly, a matrix wave equation for the magnetic field can be derived by solving Eq. (34) for the electric fields and substituting that expression into Eq. (33). The result is

$$\left\{ \begin{bmatrix} \mathbf{0} & -\mathbf{D}_{z'}^e & \mathbf{D}_{y'}^e \\ \mathbf{D}_{z'}^e & \mathbf{0} & -\mathbf{D}_{x'}^e \\ -\mathbf{D}_{y'}^e & \mathbf{D}_{x'}^e & \mathbf{0} \end{bmatrix} \begin{bmatrix} \boldsymbol{\varepsilon}_{xx}^{-1} & \mathbf{0} & \mathbf{0} \\ \mathbf{0} & \boldsymbol{\varepsilon}_{yy}^{-1} & \mathbf{0} \\ \mathbf{0} & \mathbf{0} & \boldsymbol{\varepsilon}_{zz}^{-1} \end{bmatrix} \begin{bmatrix} \mathbf{0} & -\mathbf{D}_{z'}^h & \mathbf{D}_{y'}^h \\ \mathbf{D}_{z'}^h & \mathbf{0} & -\mathbf{D}_{x'}^h \\ -\mathbf{D}_{y'}^h & \mathbf{D}_{x'}^h & \mathbf{0} \end{bmatrix} - \begin{bmatrix} \boldsymbol{\mu}_{xx} & \mathbf{0} & \mathbf{0} \\ \mathbf{0} & \boldsymbol{\mu}_{yy} & \mathbf{0} \\ \mathbf{0} & \mathbf{0} & \boldsymbol{\mu}_{zz} \end{bmatrix} \right\} \begin{bmatrix} \tilde{\mathbf{h}}_x \\ \tilde{\mathbf{h}}_y \\ \tilde{\mathbf{h}}_z \end{bmatrix} = \begin{bmatrix} \mathbf{0} \\ \mathbf{0} \\ \mathbf{0} \end{bmatrix} \quad (36)$$

In most cases, the matrices produced by 3D FDFD are prohibitively large to be solved on a standard computer by direct means like LU decomposition. In these cases, iterative algorithms [19, 20] or alternate techniques like the slice absorption method [21, 22] are recommended.

2.4. Two-Dimensional Matrix Wave Equations

Many devices can be modeled in two dimensions and this is always good practice when it can be done. This happens when devices are uniform in one direction and no wave propagation exists in the uniform direction. If the uniform direction is the z -axis, then $\mathbf{D}_{z'}^e = \mathbf{D}_{z'}^h = \mathbf{0}$ and Eqs. (20)–(25) reduce to

$$\mathbf{D}_{y'}^e \mathbf{e}_z = \boldsymbol{\mu}_{xx} \tilde{\mathbf{h}}_x \quad (37)$$

$$-\mathbf{D}_{x'}^e \mathbf{e}_z = \boldsymbol{\mu}_{yy} \tilde{\mathbf{h}}_y \quad (38)$$

$$\mathbf{D}_{x'}^e \mathbf{e}_y - \mathbf{D}_{y'}^e \mathbf{e}_x = \boldsymbol{\mu}_{zz} \tilde{\mathbf{h}}_z \quad (39)$$

$$\mathbf{D}_{y'}^h \tilde{\mathbf{h}}_z = \boldsymbol{\varepsilon}_{xx} \mathbf{e}_x \quad (40)$$

$$-\mathbf{D}_{x'}^h \tilde{\mathbf{h}}_z = \boldsymbol{\varepsilon}_{yy} \mathbf{e}_y \quad (41)$$

$$\mathbf{D}_{x'}^h \tilde{\mathbf{h}}_y - \mathbf{D}_{y'}^h \tilde{\mathbf{h}}_x = \boldsymbol{\varepsilon}_{zz} \mathbf{e}_z \quad (42)$$

After inspecting these equations, it can be seen that Maxwell's equations have decoupled into two distinct modes. The “ E -mode,” or TM polarization, is described by Eqs. (37), (38), and (42). To derive a matrix wave equation for the E -mode, Eqs. (37) and (38) are solved for the magnetic field quantities and these are substituted in Eq. (42). The results are

$$\tilde{\mathbf{h}}_x = \boldsymbol{\mu}_{xx}^{-1} \mathbf{D}_{y'}^e \mathbf{e}_z \quad (43)$$

$$\tilde{\mathbf{h}}_y = -\boldsymbol{\varepsilon}_{yy}^{-1} \mathbf{D}_{x'}^e \mathbf{e}_z \quad (44)$$

$$\left(\mathbf{D}_{x'}^h \boldsymbol{\mu}_{yy}^{-1} \mathbf{D}_{x'}^e + \mathbf{D}_{y'}^h \boldsymbol{\mu}_{xx}^{-1} \mathbf{D}_{y'}^e + \boldsymbol{\varepsilon}_{zz} \right) \mathbf{e}_z = \mathbf{0} \quad (45)$$

If desired, the magnetic fields $\tilde{\mathbf{h}}_x$ and $\tilde{\mathbf{h}}_y$ can be calculated from \mathbf{e}_z using Eqs. (43) and (44). Similarly, the “ H -mode,” or TE polarization, is described by Eqs. (39), (40), and (41). A matrix wave equation for the H -mode is derived by first solving Eqs. (40) and (41) for the electric field quantities and then substituting these expressions into Eq. (39). The results are

$$\mathbf{e}_x = \boldsymbol{\varepsilon}_{xx}^{-1} \mathbf{D}_{y'}^h \tilde{\mathbf{h}}_z \quad (46)$$

$$\mathbf{e}_y = -\boldsymbol{\varepsilon}_{yy}^{-1} \mathbf{D}_{x'}^h \tilde{\mathbf{h}}_z \quad (47)$$

$$\left(\mathbf{D}_{x'}^e \boldsymbol{\varepsilon}_{yy}^{-1} \mathbf{D}_{x'}^h + \mathbf{D}_{y'}^e \boldsymbol{\varepsilon}_{xx}^{-1} \mathbf{D}_{y'}^h + \mu_{zz} \right) \tilde{\mathbf{h}}_z = \mathbf{0} \quad (48)$$

If desired, the electric field quantities \mathbf{e}_x and \mathbf{e}_y can be computed from $\tilde{\mathbf{h}}_z$ using Eqs. (46) and (47). Both Eqs. (45) and (48) have the form $\mathbf{Ax} = \mathbf{0}$.

2.5. Summary of Formulations

All of the derivations presented in this section are summarized in Table 1. The column vector \mathbf{x} contains the electric or magnetic fields that have yet to be calculated. They are the unknown quantities. The matrix \mathbf{A} is called the wave matrix. It enforces Maxwell's equations on the fields in \mathbf{x} and contains all the information about the materials, grid, and boundary conditions. All of the matrix wave equations derived above have the general form $\mathbf{Ax} = \mathbf{0}$. This equation has only a trivial solution so it cannot be solved without incorporating a source \mathbf{b} to put the matrix equation into the form of $\mathbf{Ax} = \mathbf{b}$. The next section formulates a simple, but powerful equation that can be used to calculate this source term.

Table 1. Summary of FDFD wave matrix formulations, $\mathbf{Ax} = \mathbf{0}$.

| 3D Full Wave Formulations | | |
|--|---|---|
| $\mathbf{A}_e = \begin{bmatrix} \mathbf{0} & -\mathbf{D}_{z'}^h & \mathbf{D}_{y'}^h \\ \mathbf{D}_{z'}^h & \mathbf{0} & -\mathbf{D}_{x'}^h \\ -\mathbf{D}_{y'}^h & \mathbf{D}_{x'}^h & \mathbf{0} \end{bmatrix} \begin{bmatrix} \mu_{xx}^{-1} & \mathbf{0} & \mathbf{0} \\ \mathbf{0} & \mu_{yy}^{-1} & \mathbf{0} \\ \mathbf{0} & \mathbf{0} & \mu_{zz}^{-1} \end{bmatrix} \begin{bmatrix} \mathbf{0} & -\mathbf{D}_{z'}^e & \mathbf{D}_{y'}^e \\ \mathbf{D}_{z'}^e & \mathbf{0} & -\mathbf{D}_{x'}^e \\ -\mathbf{D}_{y'}^e & \mathbf{D}_{x'}^e & \mathbf{0} \end{bmatrix}$ $- \begin{bmatrix} \boldsymbol{\varepsilon}_{xx} & \mathbf{0} & \mathbf{0} \\ \mathbf{0} & \boldsymbol{\varepsilon}_{yy} & \mathbf{0} \\ \mathbf{0} & \mathbf{0} & \boldsymbol{\varepsilon}_{zz} \end{bmatrix}$ | $\mathbf{x}_e = \begin{bmatrix} \mathbf{e}_x \\ \mathbf{e}_y \\ \mathbf{e}_z \end{bmatrix}$ | $\mathbf{x}_h = \begin{bmatrix} \tilde{\mathbf{h}}_x \\ \tilde{\mathbf{h}}_y \\ \tilde{\mathbf{h}}_z \end{bmatrix}$ |
| $\mathbf{A}_h = \begin{bmatrix} \mathbf{0} & -\mathbf{D}_{z'}^e & \mathbf{D}_{y'}^e \\ \mathbf{D}_{z'}^e & \mathbf{0} & -\mathbf{D}_{x'}^e \\ -\mathbf{D}_{y'}^e & \mathbf{D}_{x'}^e & \mathbf{0} \end{bmatrix} \begin{bmatrix} \boldsymbol{\varepsilon}_{xx}^{-1} & \mathbf{0} & \mathbf{0} \\ \mathbf{0} & \boldsymbol{\varepsilon}_{yy}^{-1} & \mathbf{0} \\ \mathbf{0} & \mathbf{0} & \boldsymbol{\varepsilon}_{zz}^{-1} \end{bmatrix} \begin{bmatrix} \mathbf{0} & -\mathbf{D}_{z'}^h & \mathbf{D}_{y'}^h \\ \mathbf{D}_{z'}^h & \mathbf{0} & -\mathbf{D}_{x'}^h \\ -\mathbf{D}_{y'}^h & \mathbf{D}_{x'}^h & \mathbf{0} \end{bmatrix}$ $- \begin{bmatrix} \mu_{xx} & \mathbf{0} & \mathbf{0} \\ \mathbf{0} & \mu_{yy} & \mathbf{0} \\ \mathbf{0} & \mathbf{0} & \mu_{zz} \end{bmatrix}$ | $\mathbf{x}_e = \begin{bmatrix} \mathbf{e}_x \\ \mathbf{e}_y \\ \mathbf{e}_z \end{bmatrix}$ | $\mathbf{x}_h = \begin{bmatrix} \tilde{\mathbf{h}}_x \\ \tilde{\mathbf{h}}_y \\ \tilde{\mathbf{h}}_z \end{bmatrix}$ |
| 2D Formulations | | |
| $\mathbf{A}_e = \mathbf{D}_{x'}^h \mu_{yy}^{-1} \mathbf{D}_{x'}^e + \mathbf{D}_{y'}^h \mu_{xx}^{-1} \mathbf{D}_{y'}^e + \boldsymbol{\varepsilon}_{zz}$ | $\mathbf{x}_e = \mathbf{e}_z$ | $\mathbf{A}_h = \mathbf{D}_{x'}^e \boldsymbol{\varepsilon}_{yy}^{-1} \mathbf{D}_{x'}^h + \mathbf{D}_{y'}^e \boldsymbol{\varepsilon}_{xx}^{-1} \mathbf{D}_{y'}^h + \mu_{zz}$ |
| $\mathbf{A}_h = \mathbf{D}_{z'}^h \mu_{yy}^{-1} \mathbf{D}_{z'}^e + \boldsymbol{\varepsilon}_{xx}$ | $\mathbf{x}_x = \mathbf{e}_x$ | $\mathbf{A}_y = \mathbf{D}_{z'}^h \mu_{xx}^{-1} \mathbf{D}_{z'}^e + \boldsymbol{\varepsilon}_{yy}$ |
| $\mathbf{A}_y = \mathbf{D}_{z'}^e \mu_{xx}^{-1} \mathbf{D}_{z'}^h + \boldsymbol{\varepsilon}_{yy}$ | $\mathbf{x}_y = \mathbf{e}_y$ | |

3. TOTAL-FIELD/SCATTERED-FIELD FORMULATION

In this section, the TF/SF formulation is applied to derive a single equation from which \mathbf{b} can be calculated quite easily. This formulation requires all cells in the grid to be defined as either SF or TF quantities. They can be chosen arbitrarily, but usually they are chosen for convenience in post-processing and to limit energy incident on absorbing boundary conditions.

In general, two rules must be followed to successfully implement the TF/SF technique. First, the source field must be a rigorous solution to Maxwell's equations. Plane waves, cylindrical waves, and spherical waves are straightforward. Illuminating devices with beams or exciting waveguides with specific modes involve more work. Second, the source must be completely described with no ambiguity so the TF/SF interface must be a closed contour. In practice, this usually means the TF/SF interface completely surrounds the generator or cuts completely through the grid.

The finite-difference equations written for cells lying at the TF/SF interface contain both TF and SF quantities. These terms, however, are not directly compatible. For this reason, all of the finite-difference equations containing both TF and SF quantities must be corrected. The source must be added to SF quantities appearing in TF equations and subtracted from TF quantities appearing in SF equations. When this done, the correction terms are constants and can be brought to the right hand side of the matrix equation to put it in the form of $\mathbf{Ax}=\mathbf{b}$. The term \mathbf{b} is a column vector describing the source and is essentially an array containing the correction terms from all the finite-difference equations throughout the grid.

To begin deriving a simple equation to calculate \mathbf{b} , it is first necessary to compute the source field $f_{\text{src}}(x, y)$ and a masking function $Q(x, y)$ throughout the entire grid. The source field $f_{\text{src}}(x, y)$ is calculated in the absence of the device being modeled so it should look continuous and uninterrupted everywhere. This function is then reshaped into a column vector and called \mathbf{f}_{src} . It has the following general form.

$$\mathbf{f}_{\text{src}} = \begin{bmatrix} f_{\text{src}}^{(1,1)} \\ f_{\text{src}}^{(2,1)} \\ \vdots \\ f_{\text{src}}^{(N_x, N_y)} \end{bmatrix} \quad (49)$$

The masking function $Q(x, y)$ has 1's at each point on the grid that corresponds to positions in the scattered-field and 0's at each

Eq. (54) and simplifying. The result is

$$\mathbf{b} = (\mathbf{QA} - \mathbf{AQ}) \mathbf{f}_{\text{src}} \tag{55}$$

To use this equation, it is important to remember that \mathbf{f}_{src} contains the source throughout the entire grid without the device being present. The only other information needed is the masking matrix \mathbf{Q} and the wave matrix \mathbf{A} . It is worth noting that Eq. (55) can be derived independent of the underlying numerical method that converted Maxwell’s equations to matrix form with the same result. For this reason, it is the author’s assumption that the method should be equally applicable to other numerical techniques like the finite element method [23].

4. IMPLEMENTATION OF FDFD

This section summarizes how to implement the FDFD method and how to incorporate a TF/SF source using Eq. (55). A simple example is presented here just to illustrate the method. Propagation through just free space will be modeled on a grid composed of 60×60 cells. Examples of more advanced models are provided in the next section.

Step 1 — Build the device on a Yee grid

The process of building a device onto a Yee grid is depicted in Figure 3. For illustration purposes, a device was included in this

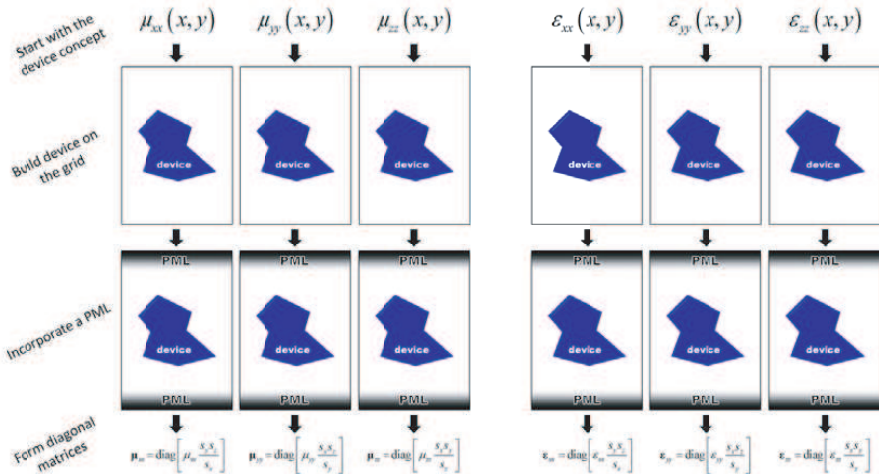


Figure 3. Constructing a device on a grid for FDFD.

figure, but only free space will be modeled here. The process begins by assigning material properties to each point in the grid. Separate functions are needed for $\mu_{xx}(x, y)$, $\mu_{yy}(x, y)$, $\mu_{zz}(x, y)$, $\varepsilon_{xx}(x, y)$, $\varepsilon_{yy}(x, y)$, and $\varepsilon_{zz}(x, y)$ because these all exist at staggered physical locations in the grid and so they can be different even for isotropic materials. These terms will differ where a material boundary passes through the middle of a cell thereby placing the staggered quantities in different materials despite being associated with the same cell. If performed correctly, visualizing the data in any of these arrays would show the device being modeled.

Next, the PML is incorporated and diagonal matrices are formed according to Eqs. (31) and (32). Here, a PML with 20 cells at the top and bottom boundaries was incorporated with parameters set to $s_{\max}=3$, $\sigma'_{\max} = 1$ and $p = 3$. For 2D simulations, no PML at the z -axis boundaries was needed so s_z was set to 1 everywhere. The square matrices $\boldsymbol{\mu}_{xx}$, $\boldsymbol{\mu}_{yy}$, $\boldsymbol{\mu}_{zz}$, $\boldsymbol{\varepsilon}_{xx}$, $\boldsymbol{\varepsilon}_{yy}$, and $\boldsymbol{\varepsilon}_{zz}$ perform point-by-point multiplications on the fields consistent with Maxwell's Equations.

Step 2 — Calculate the wave matrix \mathbf{A}

Before the wave matrix \mathbf{A} can be calculated, the derivative operators $\mathbf{D}_{x'}^e$, $\mathbf{D}_{y'}^e$, $\mathbf{D}_{z'}^e$, $\mathbf{D}_{x'}^h$, $\mathbf{D}_{y'}^h$ and $\mathbf{D}_{z'}^h$ must be constructed. It is useful to create a separate function that constructs these matrices because it will make the FDFD code cleaner and the same function can also be used in other numerical methods that use finite-differences like the method of lines [24, 25], beam propagation method [26, 27], and more [18, 21, 28]. Given the derivative operators and the diagonal materials matrices, the wave matrix \mathbf{A} is calculated using an equation from Table 1.

Step 3 — Calculate the source vector \mathbf{b}

The first step for incorporating a source is to calculate the source field $f_{\text{src}}(x, y)$ throughout the entire grid as if the device was not present. In this manner, the source field should not appear scattered. The source can be a plane wave, a cylindrical wave, a modal source, multiple sources, or virtually anything else. The source field for a plane wave incident at angle θ is calculated according to Eq. (56) and the real part is plotted in Figure 4(left) for $\theta = 30^\circ$.

$$f_{\text{src}}(x, y) = \exp[-jk_0n(x \sin \theta + y \cos \theta)] \quad (56)$$

A column vector containing the source is then constructed by reshaping the source function $f_{\text{src}}(x, y)$ into a linear array according to Eq. (49).

The next step is to construct the masking matrix \mathbf{Q} . A straightforward approach is to first build a masking function $Q(x, y)$ that is the same size and shape as the materials grid. Second, assign 1's

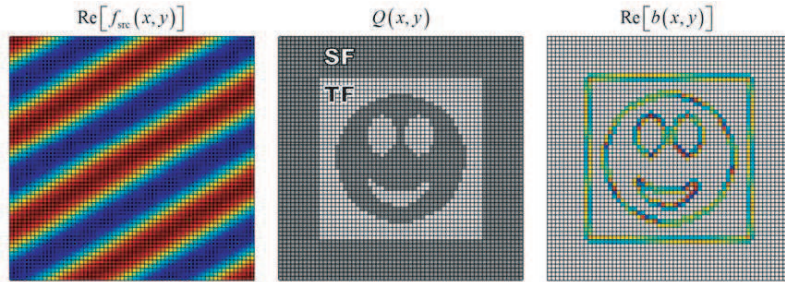


Figure 4. Visualization of the data used to calculate the source vector \mathbf{b} .

to every position desired to be a SF quantity and 0's at every position desired to be a TF quantity. An example is provided in Figure 4(center) where a smiley face was included for fun and to illustrate the versatility of Eq. (55). In practice, the entire center of the grid is usually made the TF. The \mathbf{Q} matrix is constructed by reshaping the masking function $Q(x, y)$ into a linear array and placing it along the diagonal of a sparse matrix according to Eq. (50).

Now, all the parameters needed have been defined to calculate the source vector \mathbf{b} using Eq. (55). To investigate the data calculated in the source vector \mathbf{b} for this example, it was reshaped into a 2D array and the real part visualized in Figure 4(right). It is easy to see that data only exists in this array for points on the grid that lie next to the TF/SF boundary where the correction terms are needed. Incorporating all of these corrections manually or by other means is difficult, particularly for oddly shaped TF/SF regions, but it is very easy and straightforward using Eq. (55).

Step 4 — Calculate the field \mathbf{x}

After the three steps above have been completed, the matrix equation $\mathbf{Ax}=\mathbf{b}$ can be solved for \mathbf{x} to calculate the fields.

$$\mathbf{x} = \mathbf{A}^{-1}\mathbf{b} \quad (57)$$

For most problems, this can be solved directly by LU decomposition or in MATLAB using backward division. For 3D problems, the column vector \mathbf{x} is composed of three column vectors representing the three field components. These must be parsed from \mathbf{x} before proceeding. The fields can then be reshaped from column vectors to 2D or 3D arrays so that they can be visualized or post-processed in a more straightforward manner.

The real part of the field \mathbf{x} resulting from this simple example is

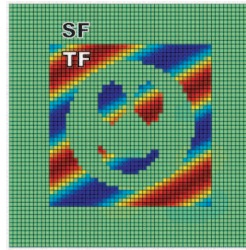


Figure 5. Real part of the field as calculated from the data shown in Figure 4.

plotted in Figure 5. Since the grid had no devices present, there were no scattered waves so all the fields in the grid defined to be in the SF region were zero. Waves are clearly present in all of the cells defined to contain TF quantities.

Step 5 — Post-process the data

It is not feasible to outline all the possible ways of post processing the field to calculate meaningful quantities. A common calculation is the overall reflectance and transmittance from a periodic device and this will be outlined here for 2D simulations. This starts by extracting the field in a “reflection record plane” and a “transmission record plane.” The reflection record plane is located at the top of the grid inside the scattered-field, but outside of the PML. The transmission record plane is located at the bottom of the grid just above the bottom PML. The materials in the record planes are typically kept homogeneous to make power calculations in those layers easier. Spacer regions were added between the device and the PML because most PML formulations do a poor job attenuating evanescent fields [29]. The spacer regions allow the evanescent field to sufficiently decay before entering the PML. This overall grid scheme is illustrated in Figure 6.

One approach to calculate overall reflectance and transmittance is to integrate the z component of the Poynting vector across the reflection and transmission record planes. While simple and straightforward to implement, this calculation does not lend itself to calculating power in each of the diffracted modes that may exist. The approach outlined below computes the overall reflectance and transmittance by first calculating the fraction of power in each diffracted mode and then adding these together to arrive at the overall reflectance and transmittance.

First, the fields are extracted from the grid at the reflection and transmission record planes. At the same time, the phase tilt $\phi(x)$ due

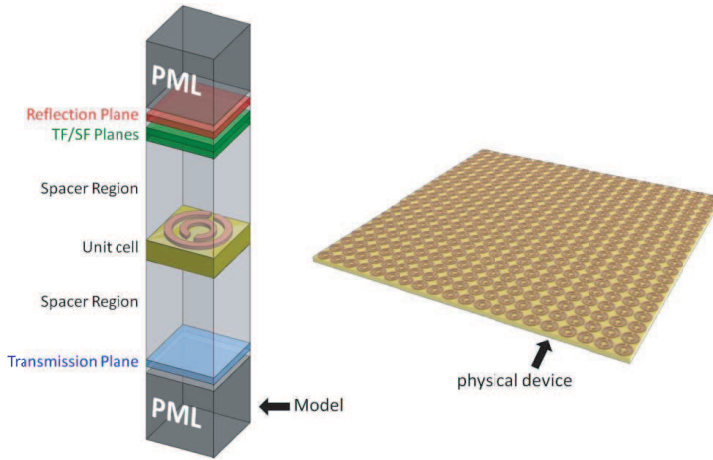


Figure 6. Typical grid scheme for periodic structures.

to an oblique angle of incidence is removed to isolate the amplitude part of the field described by Bloch's theorem [30] in periodic structures.

$$\phi(x) = \exp(-jk_{x,\text{inc}}x) \quad (58)$$

$$A_{\text{ref}}(x) = E_z(x, y_{\text{ref}}) \div \phi(x) \quad (59)$$

$$A_{\text{trn}}(x) = E_z(x, y_{\text{trn}}) \div \phi(x) \quad (60)$$

Next, the amplitudes of the diffracted waves are calculated by Fourier transforming the field from above. The diffraction order is given by the integer m .

$$S_{\text{ref}}(m) = \text{FFT}[A_{\text{ref}}(x)] \quad (61)$$

$$S_{\text{trn}}(m) = \text{FFT}[A_{\text{trn}}(x)] \quad (62)$$

The transverse wave vector components associated with each of the diffracted orders are calculated according to

$$k_{x,m} = k_x^{\text{inc}} - \frac{2\pi m}{\Lambda_x} \quad (63)$$

These terms remain the same throughout the entire grid regardless of the materials. The terms that do vary through the grid are the longitudinal components of the wave vectors associated with the diffraction orders. These can be computed from the dispersion relation, but the only time these are needed is when the transmittance and reflectance is being calculated. For this reason, they only need to be calculated in the transmission and reflection record planes according

to

$$k_{z,m}^{\text{ref}} = \sqrt{k_0^2 \mu_{r,\text{ref}} \varepsilon_{r,\text{ref}} - k_{x,m}^2} \quad (64)$$

$$k_{z,m}^{\text{trn}} = \sqrt{k_0^2 \mu_{r,\text{trn}} \varepsilon_{r,\text{trn}} - k_{x,m}^2} \quad (65)$$

Finally, given the amplitude of the incident wave S_{inc} , the power in each of the diffracted modes can be calculated. If the amplitudes of the diffracted modes were calculated from electric field quantities, power in the diffracted modes is computed according to

$$R_e(m) = \frac{|S_{\text{ref}}(m)|^2}{|S_{\text{inc}}|^2} \text{Re} \left[\frac{k_{z,m}^{\text{ref}}}{k_z^{\text{inc}}} \right] \quad (66)$$

$$T_e(m) = \frac{|S_{\text{trn}}(m)|^2}{|S_{\text{inc}}|^2} \text{Re} \left[\frac{k_{z,m}^{\text{trn}}}{k_z^{\text{trn}}} \frac{\mu_{r,\text{inc}}}{\mu_{r,\text{trn}}} \right] \quad (67)$$

If the amplitudes of the diffracted modes were calculated from magnetic field quantities, power in the diffracted modes is computed according to

$$R_h(m) = \frac{|S_{\text{ref}}(m)|^2}{|S_{\text{inc}}|^2} \text{Re} \left[\frac{k_{z,m}^{\text{ref}}}{k_z^{\text{inc}}} \right] \quad (68)$$

$$T_h(m) = \frac{|S_{\text{trn}}(m)|^2}{|S_{\text{inc}}|^2} \text{Re} \left[\frac{k_{z,m}^{\text{trn}}}{k_z^{\text{trn}}} \frac{\varepsilon_{r,\text{inc}}}{\varepsilon_{r,\text{trn}}} \right] \quad (69)$$

The overall reflectance and transmittance is the sum of the power in the diffraction orders.

$$\text{Reflectance} = \sum_m R(m) \quad (70)$$

$$\text{Transmittance} = \sum_m T(m) \quad (71)$$

If no loss or gain was incorporated into the model, the reflectance and transmittance should add to be 100%. This is an excellent check to perform at the end of the simulation. Numerical error in FDFD should not deviate from conservation of energy by more than 1%. Deviations on the order of 0.1% and 0.01% are typical.

$$\sum_m R(m) + \sum_m T(m) = \begin{cases} < 100\% & \text{materials have loss} \\ \sim 100\% & \text{no loss and no gain} \\ > 100\% & \text{materials have gain} \end{cases} \quad (72)$$

5. APPLICATIONS

The following sections provide some practical applications of Eq. (55) and how it is used to implement a TF/SF source in the FDFD method.

5.1. Periodic Structures

A basic and common simulation problem is transmission and reflection from a periodic device like a grating, frequency selective surface, or metamaterial. To illustrate the implementation in FDFD, a diffraction grating in free space was simulated with period $\Lambda = 0.9\lambda_0$, grating depth $d = 0.5\lambda_0$, substrate thickness $t = 0.5\lambda_0$, dielectric constant $\varepsilon_r = 6.0$, and duty cycle 50%. The device on the grid $\varepsilon_r(x, y)$, source field $f_{\text{src}}(x, y)$, masking function $Q(x, y)$, and resulting field $E_z(x, y)$ are shown in Figure 7. This simulation used periodic boundary conditions at the left and right boundaries and Dirichlet boundary conditions with a PML at the top and bottom boundaries. The PML size was set to 20 cells and the grid resolution was set to $\lambda/10$ for the figure. The masking function $Q(x, y)$ was designed to place only the top PML plus one additional row of cells in the SF region. The extra row of cells is where the reflected field was recorded and processed to calculate reflection.

After running a second simulation at a higher grid resolution of $\lambda/40$, the overall reflectance was calculated to be 42% and the transmittance was 58%. The same simulation was performed with rigorous coupled-wave analysis [31–33] using 121 spatial harmonics which found the reflectance to be 41% and transmittance 59%. This error of roughly 1% is not caused by the TF/SF framework. It is due to the finite-difference approximations and reflections from the PML. This is easily shown by using higher grid resolution and larger PMLs. At a grid resolution of $\lambda/120$ and 40 points in the PML regions, the FDFD method converges almost exactly to that of RCWA.

5.2. Waveguide Simulations

The TF/SF method presented in this work can be used to inject modal sources into waveguides or other structures. An example simulation and associated parameters are provided in Figure 8. Here, a slab waveguide is terminated with an anti-reflection structure by angling the end face. Figure 8(a) shows the materials for this problem placed onto the grid. The thickness of the core was set to $0.75\lambda_0$ and the overall thickness of the entire slab was set to $2\lambda_0$. The angled termination was centered in the grid. Figure 8(b) shows the source field. In this case, the “device” is the angled termination so the source was

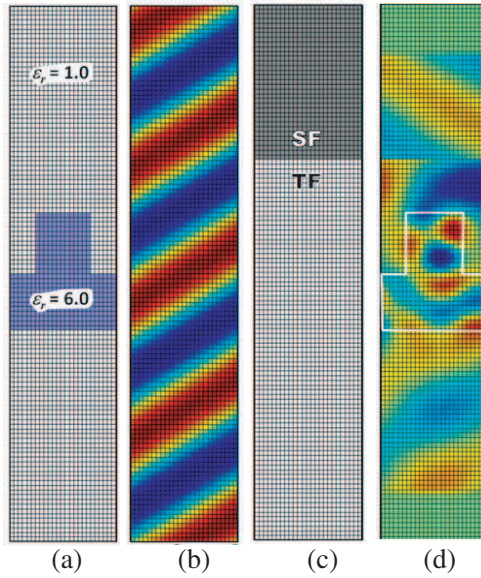


Figure 7. FDFD simulation of a plane wave source incident on a grating. (a) $\epsilon_r(x, y)$. (b) $\text{Re}[f_{\text{src}}(x, y)]$. (c) $Q(x, y)$. (d) $\text{Re}[E_z(x, y)]$.

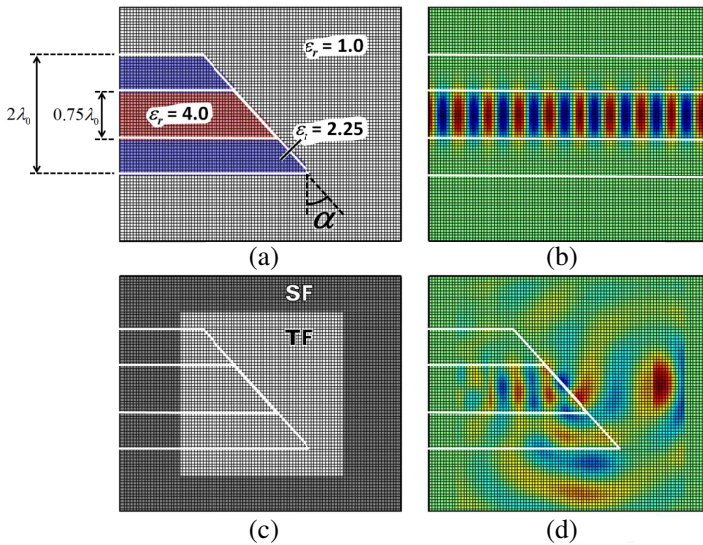


Figure 8. FDFD simulation with a modal source in a waveguide. (a) $\epsilon_r(x, y)$. (b) $\text{Re}[f_{\text{src}}(x, y)]$. (c) $Q(x, y)$. (d) $\text{Re}[E_z(x, y)]$.

calculated as if the waveguide extended all the way across the grid. Figure 8(c) shows the masking function $Q(x, y)$ where the PMLs were made to be in SF regions to minimize energy incident on them. The TF region completely encapsulated the angled termination. Finally, Figure 8(d) shows the calculated field. At a grid resolution of $\lambda/60$, it was calculated that 1.8% of the energy was reflected by the termination back into the fundamental mode when the angle of the termination was set to $\alpha = 42^\circ$ from vertical.

Several modifications to the basic FDFD algorithm were needed to perform this simulation. First, it was necessary to calculate the fundamental mode in the waveguide. To calculate a mode that is compatible with FDFD, the finite-difference method was also used to solve the cross section of the waveguide as a generalized eigen-value problem. To do this, the cross section of the waveguide was extracted from the array shown in Figure 8(a) and placed along the diagonal of the sparse matrices $\boldsymbol{\mu}'_{xx}$, $\boldsymbol{\mu}'_{yy}$, $\boldsymbol{\mu}'_{zz}$, $\boldsymbol{\epsilon}'_{xx}$, $\boldsymbol{\epsilon}'_{yy}$, and $\boldsymbol{\epsilon}'_{zz}$. The prime superscripts indicate these are 1D cross sections of the 2D grid and different from the original materials matrices calculated by Eqs. (31) and (32). The generalized eigen-value equations for the E - and H -modes are

$$\left(\mathbf{D}_{x'}^h \boldsymbol{\mu}'_{zz}{}^{-1} \mathbf{D}_{x'}^e + \boldsymbol{\epsilon}'_{yy} \right) \mathbf{e}_z = n_{\text{eff}}^2 \boldsymbol{\mu}'_{xx}{}^{-1} \mathbf{e}_z \quad (73)$$

$$\left(\mathbf{D}_{x'}^e \boldsymbol{\epsilon}'_{zz}{}^{-1} \mathbf{D}_{x'}^h + \boldsymbol{\mu}'_{yy} \right) \tilde{\mathbf{h}}_z = n_{\text{eff}}^2 \boldsymbol{\epsilon}'_{xx}{}^{-1} \tilde{\mathbf{h}}_z \quad (74)$$

Two square matrices are produced during the iterative solution of either of these equations. The eigen-vector matrix \mathbf{V} contains in its columns all of the field configurations that can exist in the cross section of the 2D grid. Some of these eigen-modes are guided modes in the slab. A diagonal eigen-value matrix $\mathbf{N}_{\text{eff}}^2$ contains the calculated eigen-values, which in this case are the squares of the effective refractive indices of the eigen-modes. The fundamental mode can be identified as having the effective refractive index closest to the refractive index of the core, $n_{\text{eff}}^2 \approx \epsilon_{\text{core}} = 4.0$. The true effective refractive index was found to be $n_{\text{eff}} = 1.94$.

Let m be the column in \mathbf{V} containing the identified fundamental mode. The source is set to equal to this column as $E_{\text{src}}(y) = \mathbf{V}(m)$. It follows that the effective refractive index is $n_{\text{eff}} = \mathbf{N}_{\text{eff}}(m)$. From this data, the sourced field is calculated all the way across the grid as if the slab waveguide was uniform. This is illustrated in Figure 8(b).

$$f_{\text{src}}(x, y) = E_{\text{src}}(y) \cdot \exp(-jk_0 n_{\text{eff}} x) \quad (75)$$

Calculation of the masking function $Q(x, y)$ and the resulting field are straightforward and the results are shown in Figures 8(c) and (d).

It was necessary to leave a column of cells between the left side PML and the TF/SF boundary. This is the plane where the reflected field $E_{\text{ref}}(y)$ was extracted. To calculate the fraction of energy reflected by the termination back into the fundamental mode, it was necessary to determine the energy in the fundamental mode given the reflected field observed in this plane. This was accomplished using the concept of mode coefficients. For the E -mode, the electric field \mathbf{e}'_z in a cross section of the grid can be written as a weighted sum of the eigen-modes in \mathbf{V} . The column vector containing these weights is \mathbf{c} and its relation to the electric field \mathbf{e}'_z that exists in the cross section is

$$\mathbf{e}'_z = \mathbf{V}\mathbf{c} \quad (76)$$

The mode coefficients of the source and reflected waves were calculated from Eq. (76) as

$$\mathbf{c}_{\text{src}} = \mathbf{V}^{-1}\mathbf{e}'_{z,\text{src}} \quad (77)$$

$$\mathbf{c}_{\text{ref}} = \mathbf{V}^{-1}\mathbf{e}'_{z,\text{ref}} \quad (78)$$

Finally, the reflectance in the fundamental mode is calculated as

$$R_0 = \left| \frac{\mathbf{c}_{\text{ref}}(m)}{\mathbf{c}_{\text{inc}}(m)} \right|^2 \quad (79)$$

5.3. Cylindrical Sources

The TF/SF method can also be used to inject cylindrical sources. Objects illuminated by sources that are in close proximity are sometimes more accurately modeled using cylindrical waves. To do this, the SF region should completely enclose the dipole generator producing the cylindrical wave. If the generator is outside of the grid, the cylindrical wave source can be treated just like a plane wave source. A simple example is depicted in Figure 9 where a cylindrical wave illuminates a square dielectric object placed in free space. Plots (a)–(d) show a first case where the simulation was performed without the object on the grid. Plots (e)–(h) show the same simulation, but with the square object placed onto the grid. The dielectric square was made to have dimension $0.6\lambda_0$ and dielectric constant $\epsilon_r = 6.0$. It was positioned in the lower right part of the grid. A dipole generator was placed in the upper left of the grid. The source field was calculated throughout the entire grid according to the following equation where the generator was centered at position (x_0, y_0) .

$$f_{\text{src}}(x, y)|_{\text{cylindrical}} = \frac{\exp(-jkr)}{\sqrt{r}} \quad r = \sqrt{(x - x_0)^2 + (y - y_0)^2} \quad (80)$$

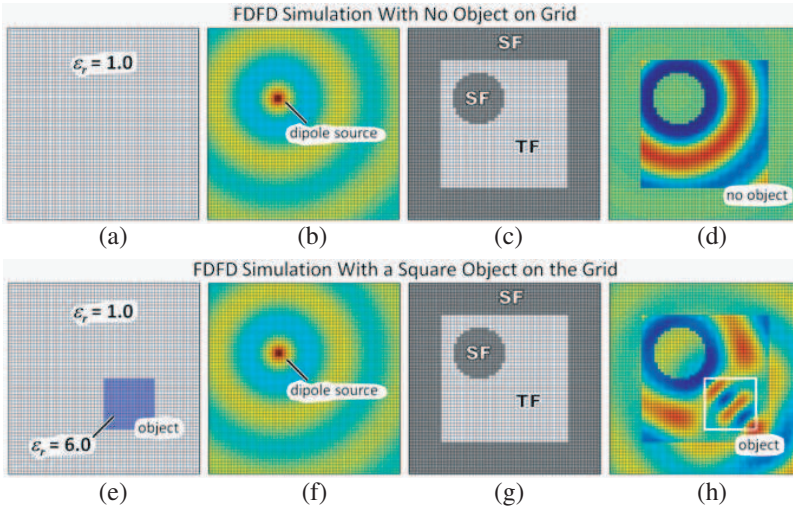


Figure 9. FDFD simulations using a cylindrical source. (a) $\varepsilon_r(x, y)$. (b) $\text{Re}[f_{\text{src}}(x, y)]$. (c) $Q(x, y)$. (d) $\text{Re}[E_z(x, y)]$. (e) $\varepsilon_r(x, y)$. (f) $\text{Re}[f_{\text{src}}(x, y)]$. (g) $Q(x, y)$. (h) $\text{Re}[E_z(x, y)]$.

For this case, $k = k_0$ is the free space wave number because the dipole generator resides in free space, not inside a material. The source field is shown in (b) and (f) and is the same for both cases. The masking function $Q(x, y)$ was defined to place the PMLs in the SF region as well as to encircle the dipole generator with the scattered field. All other points were made to be TF quantities. The $Q(x, y)$ function across the grid is visualized in (c) and (g) and was the same for both cases.

The fields were calculated and are shown in (d) and (h). For the case with no object present, the cylindrical wave is observed only in the TF regions. No field was observed in the scattered-field regions because there was no object to scatter waves. For the second case, waves were clearly present in the scattered-field regions. These are the waves that were scattered by the square object.

6. CONCLUSIONS

The TF/SF technique is a versatile method for incorporating sources into an electromagnetic model. It can be used to minimize power incident on absorbing boundary conditions and to automatically separate the source from scattered waves for easier post-processing. In FDFD, its implementation requires modifications to all of the finite-

difference equations that contain terms from both the TF and SF regions. Incorporating all of these corrections is a difficult and tedious task, particularly for oddly shaped TF/SF regions. In this paper, a simple and powerful equation was derived to perform this task in a very easy and straightforward manner. First, Maxwell's equations were converted to matrix form $\mathbf{Ax}=\mathbf{0}$ using the finite-difference method. Second, the source vector \mathbf{b} was calculated using the main equation derived in this paper to put the matrix equation in the form of $\mathbf{Ax}=\mathbf{b}$. This step automatically implemented the TF/SF framework for any shape TF and SF regions. The complete matrix equation was then solved according to $\mathbf{x}=\mathbf{A}^{-1}\mathbf{b}$ to calculate the field \mathbf{x} . A variety of practical examples were given to demonstrate the implementation and illustrate the method's power, simplicity and versatility. These included a periodic structure, a waveguide problem, and a scattering problem with a cylindrical source.

REFERENCES

1. Sun, W., K. Liu, and C. A. Balanis, "Analysis of singly and doubly periodic absorbers by frequency-domain finite-difference method," *IEEE Trans. on Antennas and Propagation*, Vol. 44, No. 6, 798–805, 1996.
2. Wu, S.-D. and E. N. Glytsis, "Volume holographic grating couplers: rigorous analysis by use of the finite-difference frequency-domain method," *Applied Optics*, Vol. 43, No. 4, 1009–1023, 2004.
3. Luo, G. Q., W. Hong, Z.-C. Hao, B. Liu, W. D. Li, J. X. Chen, H. X. Zhou, and K. Wu, "Theory and experiment of novel frequency selective surface based on substrate integrated waveguide technology," *IEEE Trans. on Antennas and Propagation*, Vol. 53, No. 12, 4035–4043, 2005.
4. Rumpf, R. C., "Design and optimization of nano-optical elements by coupling fabrication to optical behavior," Ph.D. Dissertation, 60–84, University of Central Florida, 2006.
5. Merewether, D. E., R. Risher, and F. W. Smith, "On implementing a numeric Huygen's source scheme in a finite difference program to illuminate scattering bodies," *IEEE Trans. on Nuclear Science*, Vol. 27, 1829–1833, 1980.
6. Umashankar, K. R. and A. Taflove, "A novel method to analyze electromagnetic scattering of complex objects," *IEEE Trans. on Electromagn. Compat.*, Vol. 24, 397–405, 1982.

7. Taflove, A. and S. Hagness, *Computational Electrodynamics: The Finite-difference Time-domain Method*, 3rd edition, 186–220, Artech House, Boston, 2005.
8. Sacks, Z. S., D. M. Kinsland, R. Lee, and J.-F. Lee, “A perfectly matched anisotropic absorber for use as an absorbing boundary condition,” *IEEE Trans. on Antennas and Propagation*, Vol. 43, No. 12, 1460–1463, 1995.
9. Marengo, E. A., C. M. Rappaport, and E. L. Miller, “Optimum PML ABC conductivity profile in FDFD,” *IEEE Trans. On Magnetism*, Vol. 35, No. 3, 1506–1509, 1999.
10. Arft, C. M. and A. Knoesen, “Alternatives to the perfectly matched layer for waveguide simulation using the FDFD method,” *Electromagnetics*, Vol. 25, No. 3, 177–186, 2005.
11. Bérenger, J.-P., *Perfectly Matched Layer (PML) for Computational Electromagnetics*, Morgan & Claypool, 2007.
12. Balanis, C. A., *Advanced Engineering Electromagnetics*, 1–31, Wiley, New York, 1989.
13. Yee, K. S., “Numerical solution of initial boundary value problems involving Maxwell’s equations in isotropic media,” *IEEE Trans. on Antennas and Propagation*, Vol. 14, No. 3, 302–307, 1966.
14. Taflove, A. and S. Hagness, *Computational Electrodynamics: The Finite-difference Time-domain Method*, 3rd edition, 58–84, Artech House, Boston, 2005.
15. Rumpf, R. C., “Design and optimization of nano-optical elements by coupling fabrication to optical behavior,” Ph.D. Dissertation, 72–74, University of Central Florida, 2006.
16. Yinchao, C., K. Sun, B. Beker, and R. Mittra, “Unified matrix presentation of Maxwell’s and wave equations using generalized differential matrix operators,” *IEEE Trans. on Education*, Vol. 41, No. 1, 61–69, 1998.
17. Zhu, Z. and T. G. Brown, “Full-vectorial finite-difference analysis of microstructured optical fibers,” *Optics Express*, Vol. 10, No. 17, 853–864, 2002.
18. Guo, S., F. Wu, and S. Albin, “Photonic band gap analysis using finite-difference frequency-domain method,” *Optics Express*, Vol. 12, No. 8, 1741–1746, 2004.
19. Sharkawy, M. H., V. Demir, and A. Z. Elsherbeni, “Plane wave scattering from three dimensional multiple objects using the iterative multiregion technique based on the FDFD method,” *IEEE Trans. on Antennas and Propagation*, Vol. 54, No. 2, 666–673, 2006.

20. Wu, S.-D. and E. N. Glytsis, "Finite-number-of-periods holographic gratings with finite-width incident beams: Analysis using the finite-difference frequency-domain method," *J. Opt. Soc. Am. A*, Vol. 19, No. 10, 2018–2029, 2002.
21. Rumpf, R. C., A. Tal, and S. M. Kuebler, "Rigorous electromagnetic analysis of volumetrically complex media using the slice absorption method," *J. Opt. Soc. Am. A*, Vol. 24, No. 10, 3123–3134, 2007.
22. Tal, A., Y.-S. Chen, H. E. Williams, R. C. Rumpf, and S. M. Kuebler, "Fabrication and characterization of three-dimensional copper metallodielectric photonic crystals," *Optics Express*, Vol. 15, No. 26, 18283–18293, 2007.
23. Jin, J. and J.-M. Jin, *The Finite Element Method in Electromagnetics*, 2nd edition, Vol. 1, Wiley, New York, 2002.
24. Helfert, S. F. and R. Pregla, "The method of lines: A versatile tool for the analysis of waveguide structures," *Electromagnetics*, Vol. 22, 615–637, Taylor & Francis, New York, 2002.
25. Jamid, H. A. and M. N. Akram, "Analysis of deep waveguide gratings: An efficient cascading and doubling algorithm in the method of lines framework," *J. Lightwave Technol.*, Vol. 20, No. 7, 1204–1209, 2002.
26. Lee, S. M., "Finite-difference vectorial-beam-propagation method using Yee's discretization scheme for modal fields," *J. Opt. Soc. Am. A*, Vol. 13, No. 7, 1369–1337, 1996.
27. Cherif, R., M. Zghal, R. Chatta, and C. B. Neila, "Full vector beam propagation method modeling of dual core photonic crystal fibre couplers," *Proc. SPIE*, Vol. 6182, 2006.
28. Fallahkhair, A. B., K. S. Li, and T. E. Murphy, "Vector finite difference modesolver for anisotropic dielectric waveguides," *J. Lightwave Technol.*, Vol. 26, No. 11, 1423–1431, 2008.
29. Berenger, J.-P., "Evanescent waves in PML's: Origin of the numerical reflection in wave-structure interaction problems," *IEEE Trans. on Antennas and Propagation*, Vol. 47, No. 10, 1497–1503, 1999.
30. Ashcroft, N. W and N. D. Mermin, *Solid State Physics*, Holt, Rinehart, and Winston, New York, 1976.
31. Moharam, M. G., E. B. Grann, D. A. Pommet, and T. K. Gaylord, "Formulation for stable and efficient implementation of the rigorous coupled-wave analysis of binary grating," *J. Opt. Soc. Am. A*, Vol. 12, No. 5, 1068–1076, 1995.

32. Moharam, M. G., D. A. Pommet, E. B. Grann, and T. K. Gaylord, "Stable implementation of the rigorous coupled-wave analysis for surface-relief gratings: Enhanced transmittance matrix approach," *J. Opt. Soc. Am. A*, Vol. 12, No. 5, 1077–1086, 1995.
33. Rumpf, R. C., "Design and optimization of nano-optical elements by coupling fabrication to optical behavior," Ph.D. Dissertation, 125–152, University of Central Florida, 2006.